

### **Response to the Editor's Comments**

In view of the comments of the referees, I inform you that the submitted paper could be considered for publication in *Annales Geophysicae* subject to major revisions.

Please revise your manuscript and provide a point-by-point reply to the reviewers' comments.

Thanks for the editor's warm work earnestly, we have revised the manuscript carefully according to the reviewers' comments and suggestions, please see the responses below.

The following is a point-to-point response to the reviewers' comments.

Response to Referee #1:

### **General comments**

This manuscript discusses the impact of the number of GNSS stations and the use of single/multiple GNSS constellations on the tomography results. For this purpose, this study conducts a lot of tomography experiments in Hong Kong. This study may have some reference significance, but still has some deficiencies. My major concerns are your experiment designs and key results. I have specified these points and other comments in the specific comments. In addition, the language needs significant improvement. Though I have pointed out some, there are still many other problems.

- ✓ Thanks for the reviewer's comments and suggestions, all the specific comments and suggestions have been answered point-to-point in the following. In addition, this manuscript has been proofread by a native English speaker.

### **Specific comments**

Lines 62-63: In most past studies, multi-constellation GNSS observations are simulated with ideal data which cannot reflect the real conditions of multi-constellation GNSS observations. Please be more careful to say this and check the recent publications

- ✓ Thanks for the reviewer's reminding, this expression has been revised and the corresponding descriptions of the current situation of GNSS tomography have been added, please see in P2, Lines 61-63 and Lines 66-69.

Line 159-161: The specific principle is such that: increasing the coverage rate of voxels penetrated by satellite signals and optimising the design matrix of the observation equation. This is your criterion to determine the best horizontal division of the voxels. But it is not clear to me how you assess the state of the design matrix.

- ✓ We are sorry for our improper expression, here, we want to express that the structure of design matrix can be improved by increasing the number of voxels crossed by satellite signal. Thanks for the reviewer's reminding, this expression has been revised in P5 Lines 162-165.

From lines 157-167, I cannot make a sense of what your adaptive method to determine the horizontal division is. I am also not convinced why you choose scheme 3.

- ✓ Thanks for the reviewer's question, we are sorry for our improper expression, the word 'adaptive' has been deleted. the method to determine the horizontal division is based on the principle, which guarantees the relatively large coverage rate of GNSS stations located in the bottom layer to optimize the design matrix of the observation equation, and considers a higher horizontal resolution to reflect the atmospheric water vapour distribution in as much detail as possible. For most past studies, the horizontal resolution of tomography area is selected according to the experience (e.g. 10 km, 20 km) but didn't give the reason.

- ✓ In table 1, nine schemes are given to select the horizontal resolution. Scheme 3 is determined according to the total number of divided voxels and the coverage rate of GNSS stations located in the bottom layer. Because the water vapor content is mainly concentrated on the low layers, and the tomographic result is largely affected by the distribution of GNSS observation in the low layers. Therefore, the large coverage rate of GNSS stations in the bottom layer means a large distribution of GNSS observation in the low layers, which is favorable to the final tomographic result.

Lines 227-231: I don't think the experiment and the statistics in Table 4 support your conclusion since your experiment is poorly designed and the comparison is not fair at all. I am surprised why you design such a comparison rather than single-GNSS (14 sites) vs. multi-GNSS (14 sites) and multi-GNSS (10 sites) vs. multi-GNSS (14 sites).

- ✓ We appreciate for the reviewer's suggestion, we have re-designed the comparison experiment in section 4.1, and four schemes have been designed, which are single-GNSS (10 sites), multi-GNSS (10 sites), single-GNSS (14 sites) and multi-GNSS (14 sites). In addition, all the descriptions and conclusions related to this section have been rewritten, please see in P6-9.

Line 263-265: station HKSC is near the radiosonde station, therefore, the reconstructed atmospheric wet refractivity from different cases nearby the location of radiosonde station are relatively accurate and undifferentiated. Is this because that HKSC always has enough observations? Do you use the radiosonde data of the tomographic epoch as the a priori information?

- ✓ Thanks for the reviewer's question, in our opinion, HKSC always has observations but we not sure whether it has enough observations.
- ✓ Yes, the radiosonde data of the tomographic epoch is also used as the a priori information for the location of radiosonde station, which has been described in P4 Lines135-137.
- ✓ Thanks for the reviewer's reminding, the reasons for the similar tomographic result of different cases have been revised and given in P9 Lines 263-267.

Figures 7 and 8: difficult to distinguish the different lines. Try to use more differentiable color.

- ✓ Thanks for the reviewer's suggestion, we have tried our best to distinguish the different lines using different colors in Figures 7 and 8, due to the differences between thoses schemes are small, it is very difficult to distinguish them obviously.

Table 8: the presented results surprised me. The all-GNSS scheme does not even outperform the Galileo-only scheme! I also don't think the close distance between the radiosonde station and the HKSC station can explain the negligible RMSE differences among the 9 schemes. Again, is it due to that you use the radiosonde of the tomography epoch as the a priori values?

- ✓ Yes, we totally agree with the reviewer's opinion that the similar tomographic results obtained for 9 schemes in Table 8 are related to the use of radiosonde data as the priori value for the location of radiosonde station. However, we think this may be also associated with the short distance between radiosonde and HKSC station, therefore, the reasons for the similar tomographic result of different cases have been revised and given in P9 Lines 263-267.
- ✓ In addition, a further comparison has been performed not only for the location of HKSC but also for the entire tomography area in the following part and the compared results have been presented in Figures 10 and 11 as well as in Table 9, from which it can be observed that the all-GNSS schemes are generally outperform the single-GNSS schemes.

Lines 15-16: the expression is very confusing, please be specific and accurate.

- ✓ Thanks for the reviewer's reminding, this expression has been revised in P1 Lines 15-17.

Lines.17-19: the expression is too general and inaccurate, please be specific. Try to revise it to something like "The results show that densification of the GNSS network plays a more important role than using multi-constellation GNSS observations in improving the retrieval of : : : : :".

- ✓ We appreciate for the reviewer's suggestion; this expression has been revised in P1 Lines 17-19.

Lines 19-22: the expression is redundant. "Compared to the tomographic result from the multi-constellation GNSS: : : : : when the data from the other four stations are added".

- ✓ Thanks for the reviewer's suggestion, the redundant content has been deleted.

Line 22: "more" -> "additional"

- ✓ Thanks for the reviewer's reminding, the word 'more' has been replaced by 'additional'.

Lines 26-29: unreadable expression

- ✓ Thanks for the reviewer's reminding, this expression has been revised in P1 Lines 24-27.

Line 35: delete "with which"

- ✓ Thanks for the reviewer's suggestion, the 'with which' has been deleted in the manuscript.

Line 37: "some" -> "finite" and delete "different directions"

- ✓ Thanks for the reviewer's suggestion, the word 'some' has been replaced by 'finite', and the 'different directions' has been deleted.

Line 39: “proved” -> “proven”

- ✓ Thanks for the reviewer’s suggestion, the word ‘proved’ has been replaced by ‘proven’.

Lines 42-45: poor expression

- ✓ Thanks for the reviewer’s reminding, this expression has been rewritten in P2, Lines 40-42.

Lines 47-49: try to simplify the expression and be accurate.

- ✓ Thanks for the reviewer’s reminding, this expression has been rewritten in P2, Lines 44-46.

Line 50: what does the “sparse filling” mean? Be specific

- ✓ Thanks for the reviewer’s reminding, the description of ‘sparse filling’ has been given in P2, Lines 48-49.

Lines 51-54: you never talked about “design matrix” and its link with the previously mentioned disadvantage before this expression. Though I can understand you, most readers will get lost here. Try to give a clear logic link.

- ✓ Thanks for the reviewer’s reminding, a logic link has been given using a sentence in P2, Lines 49-50.

Line 55: “modeling” -> “model”

- ✓ Thanks for the reviewer’s suggestion, the word ‘modeling’ has been replaced by ‘model’.

Line 56: delete “in which”

- ✓ We appreciate for the reviewer’s suggestion; the ‘in which’ has been deleted.

Line 59: “way of solving such” -> “way to solve this”

- ✓ Thanks for the reviewer’s suggestion, this expression has been revised.

Line 60: “increasing the density of the GNSS network: : : : :also is a : : : : :” -> “densifying the GNSS network: : : : :is another: : : : :”

- ✓ We appreciate for the reviewer’s suggestion; this sentence has been revised.

Lines 70-71: these two different things are incomparable

- ✓ Thanks for the reviewer’s reminding, this sentence has been revised in P2 Lines 72-74.

Lines 74-77: rephrase this sentence

- ✓ Thanks for the reviewer’s suggestion, this sentence has been rephrased P2 Lines 77-79.

Line 80: “detailed” -> “detailedly”

✓ Thanks for the reviewer’s comments, this expression has been revised.

Line 92: “former” -> “latter”

✓ Thanks for the reviewer’s reminding, this expression has been revised.

Line 93: “the latter” -> “the ZWD”

✓ Thanks for the reviewer’s reminding, this expression has been revised.

Line 109: delete “, and a linear expression can be listed as”, it is redundant

✓ Thanks for the reviewer’s reminding, the redundant content has been deleted.

Line 118: “not all of the unknown wet refractivity values are estimated” -> “not all of the unknowns can be determined”

✓ Thanks for the reviewer’s reminding, this expression has been revised.

Line 133: “statistically” -> “statistical”

✓ Thanks for the reviewer’s reminding, this word has been corrected.

Line 157: delete “which able”

✓ Thanks for the reviewer’s suggestion, this sentence has been revised and the word ‘which able’ has been deleted.

Line 159: delete “such”

✓ Thanks for the reviewer’s reminding, the word ‘such’ has been deleted.

Line 160: specify “coverage rate”

✓ Thanks for the reviewer’s reminding, the coverage rate has been specified in P5, Lines 167-168.

Line 188: delete “stations, as presented by triangles of different colour in Figure 1,”, redundant

✓ Thanks for the reviewer’s reminding, the redundant content has been deleted.

Line 200: delete “the”

✓ Thanks for the reviewer’s reminding, the word ‘the’ has been deleted.

Line 203: “doubled to tripled” -> “double to triple”

✓ Thanks for the reviewer’s reminding, this expression has been revised.

Line 204-205: R-14 is also evident

✓ Thanks for the reviewer’s comment, this comparison has been re-designed and all the descriptions and conclusions have been rewritten.

Line 385: “IGAR” -> “IGRA”.

✓ Thanks for the reviewer’s reminding, this expression has been revised.

Response to Referee #2:

### **General comments**

This paper examines some aspects of tropospheric tomography using GNSS signals via designed experiments. The main purpose is to investigate the impact of station density and multi-constellation systems involved in the process of estimating a better representation of water vapour in space.

### **Specific comments**

Did not quite understand the selection of the various schemes. For examples why 10 vs 14 stations? What is the basis for this choice? Do the differences between schemes in terms of RMSE as presented in Table 8 justify the main claim of the paper?

- ✓ Thanks for the reviewer's question, the selection of the various schemes in Section 4.1 have been re-designed according to the other reviewer's suggestion. Therefore, the schemes of single-GNSS (10 sites), multi-GNSS (10 sites), single-GNSS (14 sites) and multi-GNSS (14 sites) are determined to better investigate the number of GNSS rays used and coverage rate of the voxels penetrated by GNSS rays under different cases. Additionally, all the descriptions and conclusions related to this section have been rewritten, please see in P6-9.
- ✓ In our opinion, the differences between schemes in terms of RMSE as presented in Table 8 cannot justify the main claim of the paper completely, therefore, the further comparison of SWDs has been performed in the following part and the corresponding conclusion can be obtained from Figures 9 and 10 as well as Table 9.

### **Specific comments**

29 this was not as high as expected.

- ✓ Thanks for the reviewer's reminding, this expression has been revised.

37 voxels in different directions

- ✓ Thanks for the reviewer's reminding, this expression has been revised.

38 reconstructed under the assumption that the unknown

- ✓ Thanks for the reviewer's reminding, this expression has been revised.

67 GNSS data, which is the focus

- ✓ Thanks for the reviewer's reminding, this expression has been revised.

68 determine the optimal division of voxels in the horizontal direction

- ✓ Thanks for the reviewer's reminding, this expression has been revised.

70 influence of the number of stations in a network

- ✓ Thanks for the reviewer's reminding, this expression has been revised.



72 the quality and reliability of tomographic atmospheric water vapour obtained from different

✓ Thanks for the reviewer's reminding, this expression has been revised.

80 single/multi-constellation GNSS observations on troposphere tomography are analysed in detail

✓ Thanks for the reviewer's reminding, this expression has been revised.

90-94 Wrong usage of former and latter must rephrase

✓ We appreciate for the reviewer's reminding, the location of ZHD and ZWD has been exchanged.

157 In the procedure of horizontal voxel division, an approach is developed which enables the determination

✓ Thanks for the reviewer's reminding, this expression has been revised.

177 Further to the conclusion above it can also be concluded

✓ Thanks for the reviewer's reminding, this expression has been revised.

178 for the entire region using two/three/four-GNSS observations both increase with the

✓ Thanks for the reviewer's reminding, this expression has been revised.

195 following analysis focuses on: (1) investigating of two schemes in

✓ Thanks for the reviewer's reminding, this expression has been revised.

204 difference of voxels crossed by rays between Schemes 2 and 1 is not as expected for the case of

✓ Thanks for the reviewer's reminding, this expression has been revised.

219 It should be noted that the number of Galileo satellite is lower

✓ Thanks for the reviewer's reminding, this expression has been revised.

223 the highest

✓ Thanks for the reviewer's reminding, the word 'highest' has been used here.

225 only by about 3% more than

✓ Thanks for the reviewer's reminding, the word 'by' has been added.

226 of voxels for the three Schemes

✓ Thanks for the reviewer's reminding, this expression has been revised.

288 lower than that

✓ Thanks for the reviewer's reminding, the word 'smaller' has been replaced by 'lower'.

292 Hence it was

✓ Thanks for the reviewer's reminding, this word has been corrected.

323 an iterative procedure

✓ Thanks for the reviewer's question, the term 'produce' has been replaced by 'procedure'.

379 The upcoming full operability of the multi-constellation GNSS, is expected

✓ Thanks for the reviewer's suggestion, this expression has been revised.

381 results is not as expected.

✓ Thanks for the reviewer's reminding, this expression has been revised.

We appreciate for two reviewers' warm work earnestly, which has a significant improvement for our manuscript. And we hope that our corrections meet with the reviewers' requirements. Once again, thank you very much for your comments and suggestions.

# Influence of station density and multi-constellation

## GNSS observations on troposphere tomography

Qingzhi Zhao<sup>1</sup>, Kefei Zhang<sup>2,3</sup> and Wanqiang Yao<sup>1</sup>

<sup>1</sup>College of Geomatics, Xi'an University of Science and Technology, Xi'an, China.

<sup>2</sup>School of Environment Science and Spatial Informatics, China University of Mining and Technology, Xuzhou, China

<sup>3</sup>Satellite Positioning for Atmosphere, Climate and Environment (SPACE) Research Centre, RMIT University, Melbourne, Australia

**Abstract:** Troposphere tomography, using multi-constellation GNSS observations, has become a novel approach for the three-dimensional (3-d) reconstruction of water vapour fields. An analysis of the integration of four Global Navigation Satellite Systems (BeiDou, GPS, GLONASS and Galileo) observations is presented to investigate the impact of station density and single/multi-constellation GNSS observations on troposphere tomography. Additionally, the optimal horizontal resolution of the research area is determined in Hong Kong **considering both the number of voxels divided, and the coverage rate of discretized voxels penetrated by satellite signals. The results show that densification of the GNSS network plays a more important role than using multi-constellation GNSS observations in improving the retrieval of 3-d atmospheric water vapour profiles.** The RMS of SWD residuals derived from the single-GNSS observations has been decreased by 16% when the data from the other four stations are added. Furthermore, **additional** experiments have been carried out to analyse the contributions of different combined GNSS data to the reconstructed results, and the comparisons show some interesting result: (1) The number of iterations used in determining the weighting matrices of different equations in tomography modelling can be decreased when considering multi-constellation GNSS observations; (2) **the reconstructed quality of 3-d atmospheric water vapour using multi-constellation GNSS data can be improved by about 11% when compared to the PPP-estimated SWD, but this was not as high as expected.**

**Keywords:** Tropospheric tomography; Multi-constellation GNSS; Station density; Atmospheric water vapour.

## 1. Introduction

For some years, GNSS-based tropospheric tomography has been regarded as one of the most promising techniques to reconstruct the temporal-spatial variation of atmospheric water vapour (Flores et al., 2000; Grespi et al., 2008). By discretising the area of interest into **finite** voxels, the water vapour information in divided voxels can be **reconstructed under the assumption** that the unknown estimated parameters are constant during a given period (Radon, 1917; Flores et al., 2000). So far, this technique has been **proven** by some feasibility studies with GPS-only observations (Troller, 2002; Bender and Raabe, 2007; Chen and Liu, 2014) as well as the simulated multi-

38 constellation GNSS observations (Grespi et al., 2008; Bender et al., 2011; Wang et al., 2014;  
39 Benevides et al., 2015c; Benevides et al., 2017). In addition, a great improvement of tomographic  
40 result has been achieved using the multi-constellation GNSS observation when compared to that  
41 using GPS-only observations (Bender et al., 2011; Benevides et al., 2015c; Benevides et al., 2017).  
42 The geometry of the observed-signal distribution likes an inverted cone due to the fixed GNSS  
43 stations in the regional network and the distribution of satellite rays, which has a negative effect on  
44 tropospheric tomography (Benevides et al., 2015a, 2015b). The main disadvantage caused by such  
45 phenomenon is the sparse filling of the discretised voxels at the edge and lower sections of the area  
46 of interest (Bender and Raabe, 2007), and sparse filling means fewer voxels are crossed by satellite  
47 rays. Therefore, the distances are almost zero for those voxels not crossed by satellite signals, which  
48 consist the design matrix. Optimising the design matrix of observation equation is a way to  
49 overcome such bad condition by selecting a non-uniform symmetrical division of horizontal voxels  
50 and a non-uniform thickness of the vertical voxel layers (Nilsson and Gradinarsky, 2006; Yao and  
51 Zhao, 2016a, 2016b). Imposing the satellite rays which come out from the side of the research area  
52 onto the reconstructed model is another effective way to optimise the structure of the design matrix  
53 (Yao and Zhao, 2016b; Yao et al., 2016; Zhao and Yao, 2017). In addition, using more slant-path  
54 observations derived from the upcoming fully-operational GNSS constellations (BeiDou,  
55 GLONASS, and Galileo) is a possible way to solve this issue (Grespi et al., 2008; Bender et al.,  
56 2011; Benevides et al., 2017). Finally, densifying the GNSS network is another feasible way to  
57 improve the stability and structure of the design matrix (Nilsson and Gradinarsky, 2006).

58 Multi-constellation GNSS observations simulated with ideal data have been used for GNSS  
59 tomography technique, however, it cannot reflect the real conditions of multi-constellation GNSS  
60 observations, including the variations in latitudes, areas, topography, and the surroundings of GNSS  
61 stations (Nilsson and Gradinarsky, 2006; Grespi et al., 2008; Wang et al., 2014). Therefore, the  
62 preliminary result concluded from those studies needs further verification based on the observed  
63 multi-constellation GNSS data. Although some tomographic experiments have been performed  
64 using the observed multi-GNSS observations (Benevides et al., 2017; Dong et al., 2018; Zhao et al.,  
65 2018), the influence of station density and different combination of multi-GNSS observations on  
66 troposphere tomography have never been well-investigated, which is the focus of this study. In this  
67 paper, a method is proposed to determine the optimal division of voxels in the horizontal direction  
68 automatically according to the range of the tomography area as well as the number and distribution  
69 of GNSS stations. The influence of the number of stations in a network on the tomographic result  
70 and the reconstructed wet refractivity field derived from multi-GNSS observations are both analysed.  
71 Finally, the quality and reliability of tomographic atmospheric water vapour obtained from different  
72 combined multi-constellation GNSS observations is analysed.

73 The aim of this paper is to analyse the influence of station density and single/multi-constellation  
74 GNSS observations on tropospheric tomography in an upcoming future scenario of having the multi-  
75 GNSS constellations fully operated. The structure of this paper is organised as follows: Sect. II  
76 presents the theory of tropospheric tomography, Sect. III describes the experimental data and the  
77 determination of horizontal resolution. The importance and influence of station density and  
78 single/multi-constellation GNSS observations on troposphere tomography are analysed in detail and  
79 compared in Sects IV and V, respectively, and key conclusions are presented in Sect. VI.

80

## 81 2. GNSS tropospheric tomography

82 Generally, slant wet delay (SWD) and slant water vapour (SWV) are two types of input observations  
 83 used in building the observation equations, and the corresponding output results are wet refractivity  
 84 and water vapour density, respectively (Flores et al., 2000; Skone and Hoyle, 2005; Notarpietro et  
 85 al., 2011; Champollion et al., 2005). Two kinds of reconstructed output information can be inter-  
 86 converted with atmospheric temperature field information (Bender et al., 2011). In this paper, the  
 87 SWD is selected to reconstruct the atmospheric wet refractivity field.

88 The zenith tropospheric delay (ZTD) is estimated with high precision using the GNSS observation,  
 89 consists of two parts, **which includes zenith hydrostatic delay (ZHD) and zenith wet delay (ZWD)**.  
 90 The former can be accurately estimated based on the empirical model, *e.g.*, Saastamoinen (1973),  
 91 with the observed surface pressure information. Therefore, the latter is obtained by subtracting the  
 92 ZHD from ZTD. In our study, the observed multi-constellation GNSS data are processed using the  
 93 multi-constellation GNSS Precise Point Positioning (PPP) software with precise orbit and clock  
 94 error products (Zhao et al., 2018). Consequently, the SWD can be expressed as:

$$95 \quad \text{SWD}_{azi,ele} = m_w(ele) \cdot \text{ZWD} + m_w(ele) \cdot \cot(ele) \cdot (G_{NS}^w \cdot \cos(azi) + G_{WE}^w \cdot \sin(azi)) \quad (1)$$

96 Where  $m_w$  is the wet mapping function. In our processing, the wet Vienna Mapping Function  
 97 (VMF) is adopted;  $ele$  refers to the satellite elevation angle while  $azi$  represents the azimuth  
 98 angle.  $G_{NS}^w$  and  $G_{WE}^w$  are the north-south and west-east gradients of wet delay, respectively, which  
 99 are caused by the non-isotropic nature of atmospheric water vapour distributions (Bi et al., 2006).  
 100 The SWD value from the satellite to GNSS station antenna is an integral expression, given by:

$$101 \quad \text{SWD} = 10^{-6} \cdot \int N_w(s) ds \quad (2)$$

102 Where  $N_w$  represents the wet refractivity (mm/km) and  $s$  is the distance over which the satellite  
 103 signal penetrates the troposphere (km). According to this tomographic technique, the area of interest  
 104 is divided into a number of voxels and the wet refractivity parameters are considered unchanged  
 105 during the selected period. Consequently, the total SWD value can be expressed as the sum of  
 106 discretised delay parts in each voxel along the satellite ray path:

$$107 \quad \text{SWD} = \sum_{i=1}^m \sum_{j=1}^n \sum_{k=1}^p (a_{ijk} \cdot x_{ijk}) \quad (3)$$

108 Where  $m$  and  $n$  are the total number of voxels divided in longitudinal and latitudinal directions  
 109 while  $p$  is the total number in vertical direction, respectively;  $a_{ijk}$  is the distance of satellite rays,

110 and  $x_{ijk}$  is the unknown wet refractivity parameters in voxel  $(i, j, k)$ , respectively. Therefore, the  
 111 observation equation of tomography modelling can be established for all GNSS stations in a network  
 112 of interesting area.

113 As mentioned above, the geometric distribution of satellite rays in the tomographic area is an  
 114 inverted cone, thus the design matrix of observation equations is a sparse matrix and **not all of the**  
 115 **unknowns can be determined**. To solve the problem of rank deficiency, some external constraints

116 are required (Flores et al., 2000; Troller et al., 2006; Rohm and Bosy., 2011). Two constraints are  
 117 imposed in this paper, the one is the horizontal weighted constraint, and the other is the vertical  
 118 constraint based on the observed radiosonde data in the first three days of the reconstructed epoch.  
 119 Consequently, the conventional tomographic modelling imposed the following constraint equations:

$$120 \quad \begin{pmatrix} \mathbf{A} \\ \mathbf{H} \\ \mathbf{V} \end{pmatrix} \cdot \mathbf{x} = \begin{pmatrix} \mathbf{y}_{swd} \\ \mathbf{0} \\ \mathbf{y}_{rs} \end{pmatrix} \quad (4)$$

121 Where  $\mathbf{H}$  represents to the horizontal coefficient matrices while  $\mathbf{V}$  refers to the vertical  
 122 coefficient matrices, respectively.  $\mathbf{y}_{swd}$  is a vector with SWD values while  $\mathbf{y}_{rs}$  is the *a priori*  
 123 information obtained from the radiosonde information. The form of solution of the unknown wet  
 124 refractivity vector can be written as:

$$125 \quad \hat{\mathbf{x}} = (\mathbf{A}^T \cdot \mathbf{P}_A \cdot \mathbf{A} + \mathbf{H}^T \cdot \mathbf{P}_H \cdot \mathbf{H} + \mathbf{V}^T \cdot \mathbf{P}_V \cdot \mathbf{V})^{-1} \cdot (\mathbf{A}^T \cdot \mathbf{P}_A \cdot \mathbf{y}_{swd} + \mathbf{V}^T \cdot \mathbf{P}_V \cdot \mathbf{y}_{rs}) \quad (5)$$

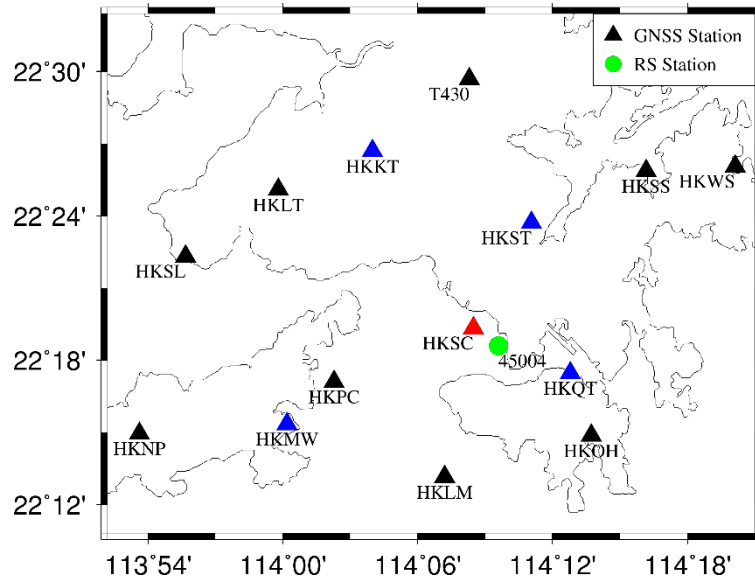
126 Where  $\mathbf{P}_A, \mathbf{P}_H$ , and  $\mathbf{P}_V$  are the weighting matrices of observation, horizontal and vertical  
 127 equation, respectively. The weighting matrices for different equations are determined by an optimal  
 128 weighting method and the homogeneity test was adopted to verify the **statistical** equality of three  
 129 kinds of *a posteriori* unit weight variances (Bartlett, 1937; Guo et al., 2016). **Here, the radiosonde**  
 130 **data of the tomographic epoch is also used as the a priori information for the location of radiosonde**  
 131 **station.**

### 133 3. Tomography experiment and description

#### 134 3.1 Experimental data

135 A network consisting of fourteen GNSS Satellite Reference Stations (SatRef) in Hong Kong was  
 136 selected to perform the tomography experiment during the period of Doy 4 to 26, 2017. The  
 137 geographic locations of GNSS and radiosonde stations are presented in Fig. 1. The sampling interval  
 138 of the GNSS observations used here was 30 s. The radiosonde station in the experimental area is  
 139 used to test the reconstructed result of GNSS troposphere tomography. The range of tomographic  
 140 region is from 113.87 °E to 114.35 °E and 22.18 °N to 22.54 °N while the vertical height is from 0  
 141 to 9 km. The horizontal resolution, in voxel terms, is  $4 \times 12$  in latitudinal and longitudinal directions  
 142 as determined by an optimal voxel division method, which will be described below. The vertical  
 143 resolution adopts a non-uniform vertical layer strategy (Yao and Zhao, 2016b) with two layers of a  
 144 thickness of 500 m, three layers of 600 m, four layers of 800 m, and three layers of 1000 m from  
 145 the ground to the top of tomography region.

146



147  
148  
149  
150  
151  
152

Fig. 1. Geographic location of GNSS and radiosonde stations in SatRef of Hong Kong. The blue triangles are used to increase the station density, while the station HKSC marked in red and radiosonde station 45004 marked in green are used to evaluate the performance of tomographic result

### 153 3.2 Determination of horizontal resolution

154 In the procedure of horizontal voxel division, an approach is developed which enables the  
155 determination of the optimal horizontal resolution according to the scope of tomography region as  
156 well as the number and distribution of GNSS stations. The specific principle is that: guaranteeing  
157 the relatively large coverage rate of GNSS stations located in the bottom layer to optimize the design  
158 matrix of the observation equation, and considering a higher horizontal resolution to reflect the  
159 atmospheric water vapour distribution in as much detail as possible, therefore, a comparative  
160 experiment is performed to validate the developed approach of determining horizontal resolution.  
161 Here, the coverage rate refers to the ratio between the voxels crossed by satellite rays and total  
162 voxels divided in the tomographic area. Nine schemes are designed (Table 1): the number of voxels  
163 for the bottom layers and the coverage rate of distributed stations located at the bottom layer are  
164 calculated. It can be concluded that Scheme 3 was optimal while considering both the number of  
165 voxels divided and the coverage rate of GNSS stations located in the bottom layers.

166

Table 1. Statistical result of determining a horizontal resolution for nine schemes

Scheme	Longitude× Latitude	Total voxels	Step of longitude	Step of latitude	Coverage rate of stations (%)
1	12×9	108	0.04	0.04	13.0
2	12×6	72	0.04	0.06	18.1
3	12×4	48	0.04	0.09	29.2
4	8×9	72	0.06	0.04	19.4
5	8×6	48	0.06	0.06	25.0
6	8×4	32	0.06	0.09	43.8
7	6×9	54	0.08	0.04	25.9
8	6×6	36	0.08	0.06	36.1

9	6×4	24	0.08	0.09	58.3
---	-----	----	------	------	------

167

168 In addition, the coverage rate of the satellite rays for the entire research region is analysed for the  
 169 date of day 4, 2017 under nine combined multi-constellation GNSS observations. In this study, the  
 170 time period for each tomography is selected as five minutes. The specific statistical result is  
 171 presented in Table 2, where G/C/R/E refer to GPS, BeiDou, GLONASS, and Galileo, respectively.  
 172 The conclusion can be drawn that the coverage rate of satellite rays in Schemes 3, 6, 8, and 9 are  
 173 relatively large. Considering the number of voxels and coverage rate of stations located in the  
 174 bottom layers, Scheme 3 is also considered as the optimal choice. **Further to the conclusion above**  
 175 **it can also be concluded** that the coverage rate of voxels penetrated by satellite signals for the entire  
 176 region using two/three/four-GNSS observations both increased with the minimum coverage rate by  
 177 approximately 5% when compared to the single-GNSS conditions.

178 Table 2. Coverage rate of satellite rays for nine combined multi-constellation GNSS observations  
 179 (Unit: %)

Scheme	1	2	3	4	5	6	7	8	9
G	51.3	60.8	72.7	61.0	69.8	81.4	67.2	76.0	85.8
C	50.0	61.2	73.9	57.4	68.5	80.6	62.2	72.6	82.5
R	44.0	54.4	67.7	53.5	62.9	78.0	61.5	71.5	84.1
E	30.9	40.3	53.1	40.0	50.6	64.9	47.0	57.7	72.1
GC	62.1	71.2	79.3	69.0	77.6	85.0	72.8	81.2	87.8
GR	60.4	68.8	79.5	68.0	75.8	85.2	73.1	80.9	88.5
CR	59.2	69.5	79.1	65.9	75.9	84.4	70.9	80.3	86.9
GCR	65.6	74.1	81.7	71.6	80.0	86.5	75.5	83.3	89.2
GCRE	66.9	75.3	82.3	72.5	80.5	86.8	76.1	83.6	89.5

180

#### 181 4. Influence of station density on tropospheric tomography

182 In this section, **four schemes** are designed to analyse the influence of station density and multi-  
 183 constellation GNSS data on the reconstructed atmospheric wet refractivity. **For Schemes 1 and 2,**  
 184 **only ten GNSS stations are used, as shown by the nine black triangles and one red triangle in Figure**  
 185 **1, but considering the single-GNSS observation and different multi-constellation GNSS**  
 186 **combinations. The single-GNSS observation is abbreviated to G-10, C-10, R-10, and E-10,**  
 187 **respectively while those combinations are abbreviated to GC-10, GR-10, CR-10, GCR-10, and**  
 188 **GCRE-10, respectively. For Schemes 3 and 4, all fourteen GNSS stations are selected for this**  
 189 **tomographic experiment but considering single-GNSS observation and different multi-constellation**  
 190 **GNSS combinations. The single-GNSS observation is abbreviated to G-14, C-14, R-14, and E-14,**  
 191 **respectively while those combinations are abbreviated to GC-14, GR-14, CR-14, GCR-14, and**  
 192 **GCRE-14, respectively.** The following analysis focussed on: (1) the investigating of four schemes  
 193 in the number of GNSS rays used and coverage rate of the voxels penetrated by GNSS rays,  
 194 respectively; (2) the comparison of reconstructed result with radiosonde data as well as the PPP-  
 195 estimated SWD values of station HKSC, respectively.



## 4.1 Comparison of GNSS rays used and the coverage rate of voxels

### penetrated

23 days of data during the period day 4-26, 2017 are analysed and Table 3 shows the mean value of GNSS rays used and coverage rate of voxels penetrated by signals for the test period. It can be concluded from the statistical results (Table 3) that the number of signals used in Schemes 2 and 4 is apparently large (double to triple) compared to that of Schemes 1 and 3, however, percentage difference of voxels crossed by rays between Schemes 1/3 and Schemes 2/4 is not as expected except for the cases of E-10 and E-14. The number of Galileo satellite observations is small during the test period, therefore, a low number of signals used and a low coverage rate of voxels penetrated by GNSS signals existed for the cases of E-10 and E-14 in Schemes 1 and 3.

Table 3. Number of GNSS rays used and the coverage rate of crossed voxels in different schemes during the experimental period

	Scheme 1				Scheme 2				
	G -10	C -10	R -10	E -10	GC -10	GR -10	CR -10	GCR -10	GCRE -10
Number of signals used	673	761	471	233	1433	1144	1232	1905	2137
Coverage rate of voxels (%)	66.6	60.8	57.3	37.0	73.8	73.6	71.2	76.9	77.4
	Scheme 3				Scheme 4				
	G -14	C -14	R -14	E -14	GC -14	GR -14	CR -14	GCR -14	GCRE -14
Number of signals used	974	1123	693	349	2097	1668	1816	2791	3139
Coverage rate of voxels (%)	75.3	71.8	68.0	50.0	80.0	79.8	78.8	82.0	82.3

\*-14 refers to the statistical result with single-GNSS observations derived from fourteen stations

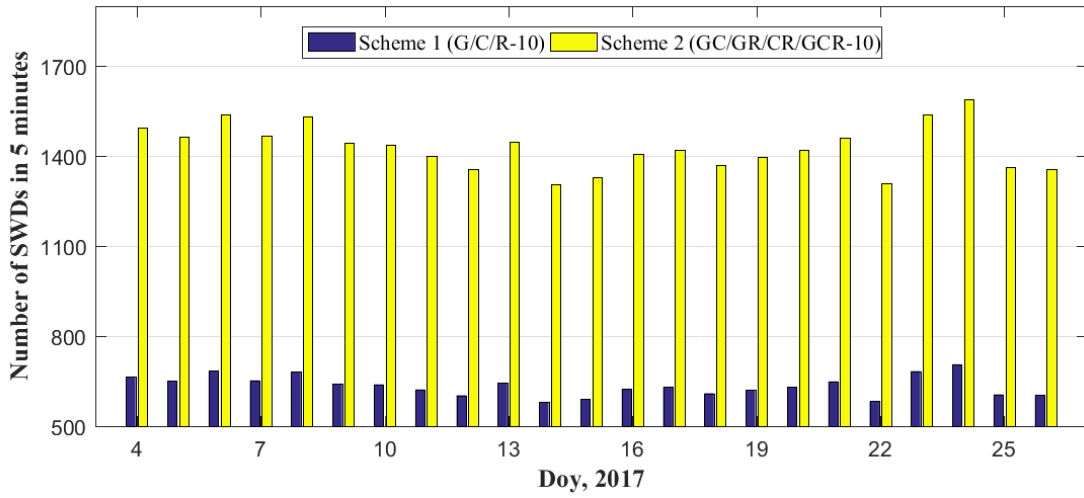
\*-10 refers to the statistical result with multi-constellation GNSS observations derived from ten stations

To analyse the number of SWDs used and the coverage rate of voxels, the average values of four schemes for each day is calculated in Figures 2-5, respectively. Due to the number of Galileo satellites is lower, therefore, the cases associated with Galileo are not considered in four schemes. Figures 2 and 4 reveals that the signals used for each day in Schemes 2 and 4 are more than double that in Schemes 1 and 3, however, Figures 3 and 5 reveals that the proportion of voxels penetrated by GNSS signals in Schemes 2 and 4 are only improved by approximately 12% and 8.7%, respectively than that in Schemes 1 and 3.

Table 4 lists statistical results relating to SWD numbers and the coverage rate of voxels for the four Schemes mentioned above. From Table 4 we concluded that although the number of satellite rays has been doubled, the percentage of crosses voxels is increased by approximately 12% and 8%, respectively for the comparisons of schemes 1 and 2 as well as schemes 3 and 4. However, the voxels crossed by rays have been improved by 10% and 6%, respectively when comparing the schemes 1 and 3 as well as schemes 2 and 4 under the conditions that only considering additional four GNSS stations for single-GNSS and multi-GNSS. This indicates that the station density has a more important influence on the coverage rate of voxels crossed by rays than multi-constellation

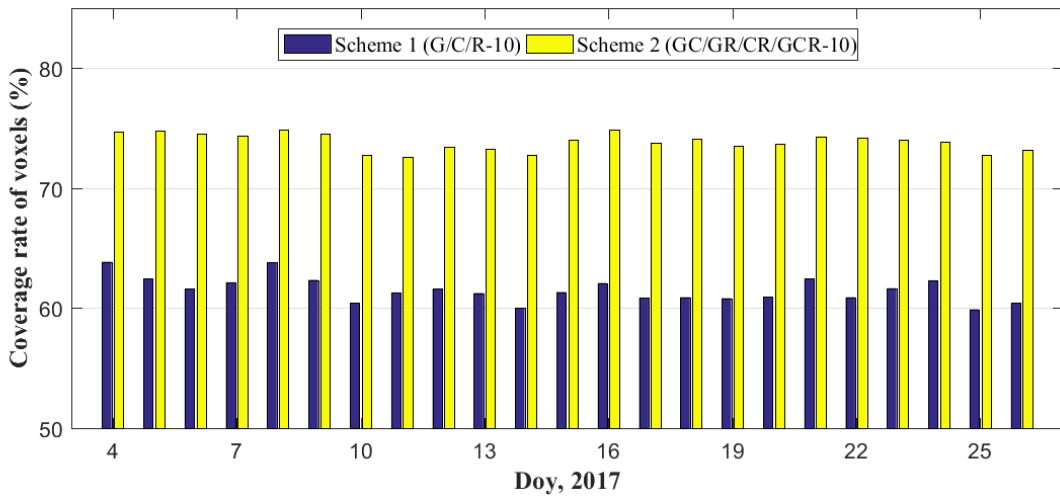
228 GNSS observations.

229



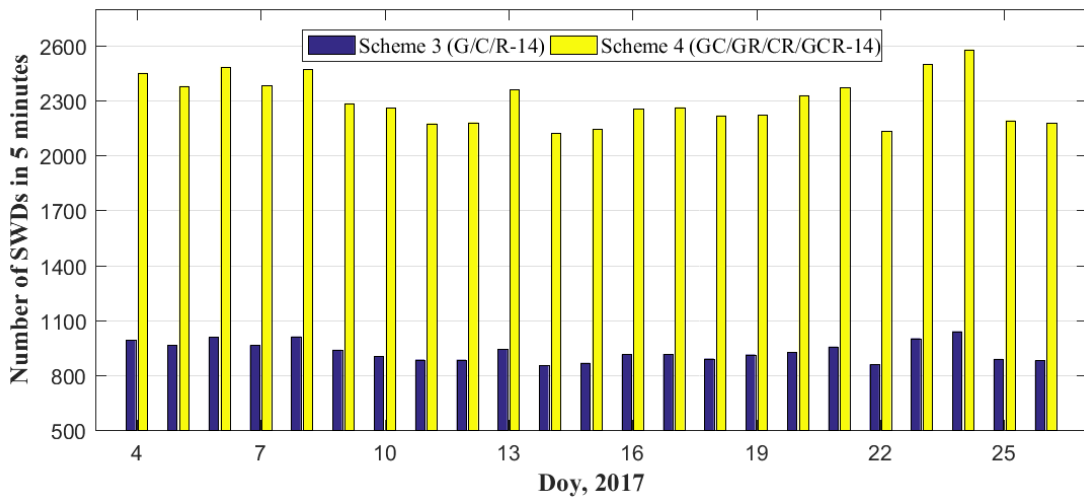
230

231 Figure 2. Average number of SWDs used in 5 minutes for Schemes 1 and 2 during the  
232 experimental period



233

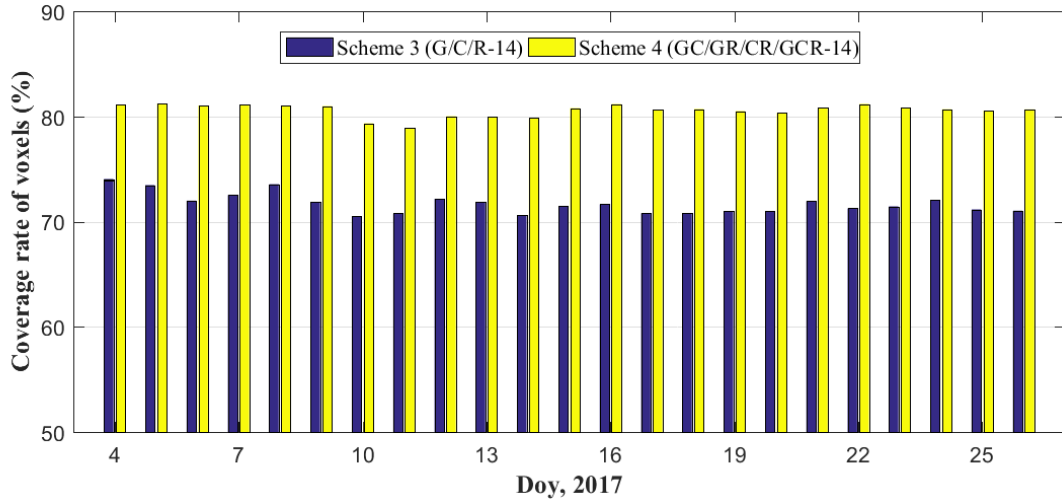
234 Figure 3. Average coverage rate of voxels penetrated by GNSS signals for Schemes 1 and 2 during  
235 the experimental period



236

237  
238  
239

Figure 4. Average number of SWDs used in 5 minutes for Schemes 3 and 4 during the experimental period



240

Figure 5. Average coverage rate of voxels penetrated by GNSS signals for Schemes 3 and 4 during the experimental period

242

Table 4. Statistical information of GNSS signals used and the percentage of voxels penetrated during the tested period for four schemes

244

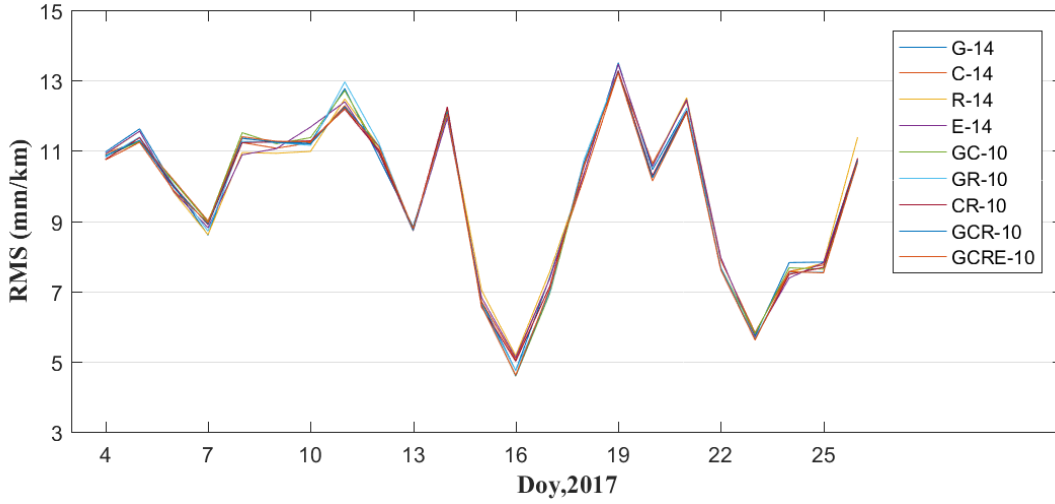
Scheme	Number of signals used	Percentage of crossed voxels (%)
1	635	61.6
2	1429	73.9
3	930	71.7
4	2093	80.2

245

## 246 4.2 Comparison with radiosonde data

247 In this section, we further compared the influence of station density on the tomographic result. In  
 248 the experimental area, there is a radiosonde station, as shown by the green circle in Figure 1. Several  
 249 studies have proved that radiosonde data has a high accuracy in providing the water vapour profiles  
 250 (Niell et al., 2001; Liu et al., 2013), and the result calculated from radiosonde is used as a reference  
 251 in this paper to evaluate the tomographic result. The comparison experiment of reconstructed wet  
 252 refractivity profile information using different GNSS observations at the radiosonde station with the  
 253 radiosonde data is carried out at two specific epochs (UTC 00:00 and 12:00, respectively). Figure 6  
 254 shows the root mean square (RMS) error of wet refractivity difference between different  
 255 tomography conditions and radiosonde data. Table 5 gives the specific statistical information  
 256 pertaining to RMS, bias, and mean absolute error (MAE) for different Schemes. From Figure 6 and  
 257 Table 5, we can conclude that the tomographic results using different single/multi-constellation  
 258 GNSS observations are similar at the radiosonde location. This is because (1) the priori information  
 259 of radiosonde has been imposed into the tomography modelling for the location of radiosonde  
 260 station; (2) station HKSC is near the radiosonde station, and a relatively large amount of GNSS  
 261 observations distributed for the location of radiosonde station. However, such a result cannot

262 represent the quality of reconstructed results of wet refractivity fields for the entire region. Therefore,  
 263 the performance of the tomographic result for the entire research region is further evaluated using  
 264 the PPP-estimated SWDs below.  
 265



266  
 267 Figure 6. RMS error of wet refractivity difference derived from various conditions during the  
 268 experiment period

269 Table 5. Statistical result of RMS, Bias and MAE of wet refractivity difference for different  
 270 Schemes during the experimental period

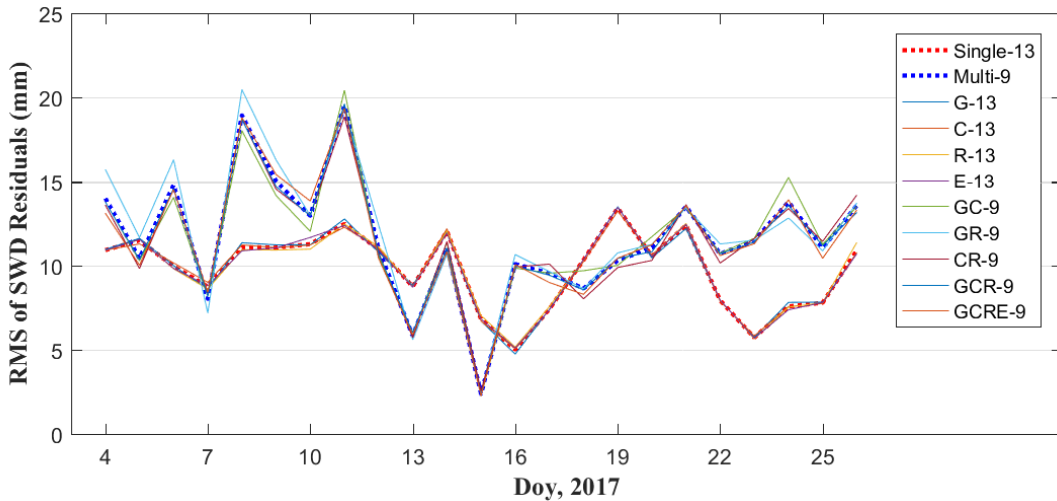
Scheme		RMS (mm/km)	Bias (mm/km)	MAE (mm/km)
Single	G-14	9.78	1.54	7.12
	C-14	9.78	1.55	7.14
	R-14	9.75	1.64	7.15
	E-14	9.76	1.66	7.14
Multi	GC-10	9.72	1.40	7.10
	GR-10	9.71	1.40	7.10
	CR-10	9.72	1.46	7.10
	GCR-10	9.68	1.41	7.07
	GCRE-10	9.66	1.42	7.07

271

### 272 4.3 Comparison with PPP-estimated SWDs

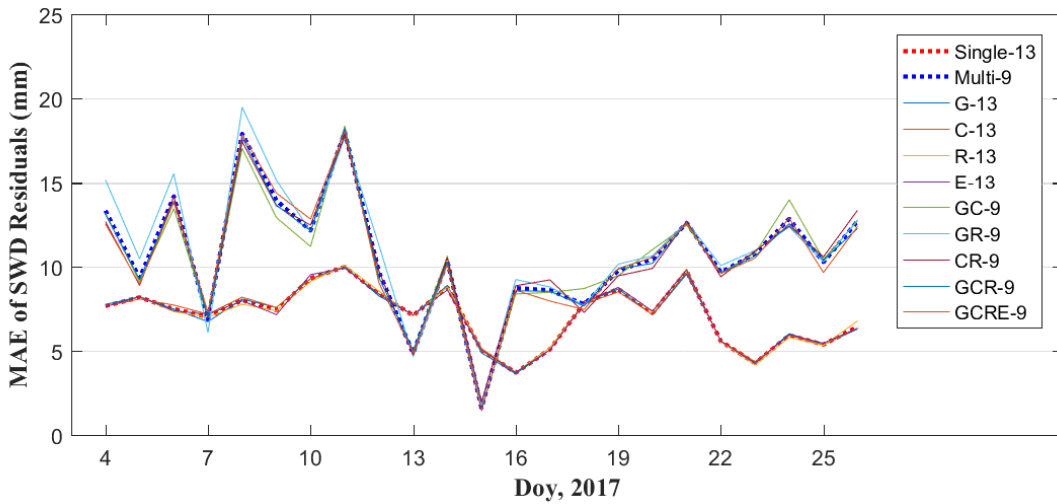
273 To assess the reconstructed result of the entire region, two new schemes are designed: Scheme 1,  
 274 only the single-GNSS observations of thirteen GNSS stations (except for HKSC) are used for  
 275 reconstructing the atmospheric wet refractivity; Scheme 2, nine GNSS stations, as shown by the  
 276 black triangles in Figure 1, are selected using combined multi-constellation GNSS observations.  
 277 The slant wet delays (SWDs) of station HKSC are computed based on the different tomographic  
 278 results and against the GNSS PPP-estimated SWDs. The RMS and MAE of SWD residuals for each  
 279 day in two schemes are presented in Figures 7 and 8, where the red dashed line represents the  
 280 average RMS and MAE obtained under conditions G-13, C-13, R-13, and E-13 while the blue  
 281 dashed line represents the average RMS and MAE obtained from cases GC-9, GR-9, CR-9, GCR-

282 9, and GCRE-9, respectively. Figures 7 and 8 reveal that the average RMS and MAE of Scheme 1  
 283 is mostly **lower** than that of Scheme 2 over the experimental period, which shows that the  
 284 reconstructed atmospheric wet refractivity field of Scheme 1 over the entire research area is superior  
 285 to the tomographic result of Scheme 2. Statistical results pertaining to different schemes are listed  
 286 in Table 6, from which it is seen that, compared to Scheme 2, the average RMS and MAE accuracy  
 287 of Scheme 1 is increased by 16% and 33.4%, respectively. **Hence** it was concluded that, compared  
 288 to the tomographic result of multi-constellation GNSS observations, increasing the station density  
 289 has greater significance to the reconstruction of the atmospheric water vapour field.  
 290



291

292 Figure 7. Average RMS of SWD residuals for different schemes over the experimental period



293

294 Figure 8. Average MAE of SWD residuals for different schemes over the experimental period

295 Table 6. Statistical result of RMS and MAE of different tomographic strategies over the  
 296 experimental period

Scheme	RMS	MAE	
Single	G-13	9.78	7.12
	C-13	9.77	7.14
	R-13	9.79	7.15
	E-13	9.76	7.14

	GC-9	11.64	10.62
	GR-9	11.99	11.09
Multi	CR-9	11.50	10.66
	GCR-9	11.55	10.61
	GCRE-9	11.52	10.58

297

## 298 5 Analysis of multi-constellation GNSS troposphere tomography

### 299 5.1 Comparison of signals used and coverage rate of voxels penetrated

300 Here, all fourteen GNSS stations are selected to reconstruct the atmospheric wet refractivity, and  
301 the tomographic results derived from different multi-constellation GNSS observations are compared  
302 and analysed. Nine types of single/multi-constellation GNSS observations are designed in schemes  
303 designated: G-14, C-14, R-14, E-14, GC-14, GR-14, CR-14, GCR-14, and GCRE-14, respectively.  
304 Before evaluating the performance of the tomographic result, the average number of GNSS signals  
305 used and the percentage of voxels penetrated over the experimental period for each tomography step  
306 are first analysed (Table 7). Table 7 reveals that compared to schemes G-14 C-14, R-14, and E-14,  
307 multi-constellation GNSS schemes have more voxels crossed by rays, but the change is relatively  
308 small with respect to the coverage rate of voxels.

309

310 Table 7. Statistical information of the number of GNSS rays used and the coverage rate of voxels  
311 penetrated

	G -14	C -14	R -14	E -14	GC -14	GR -14	CR -14	GCR -14	GCRE -14
Number of signals used	974	1123	693	349	2097	1168	1816	2791	3139
Coverage rate of voxels (%)	75.3	71.8	68.0	50.0	80.0	79.8	78.8	82.0	82.4

312

### 313 5.2 Evaluation of multi-constellation GNSS troposphere tomography

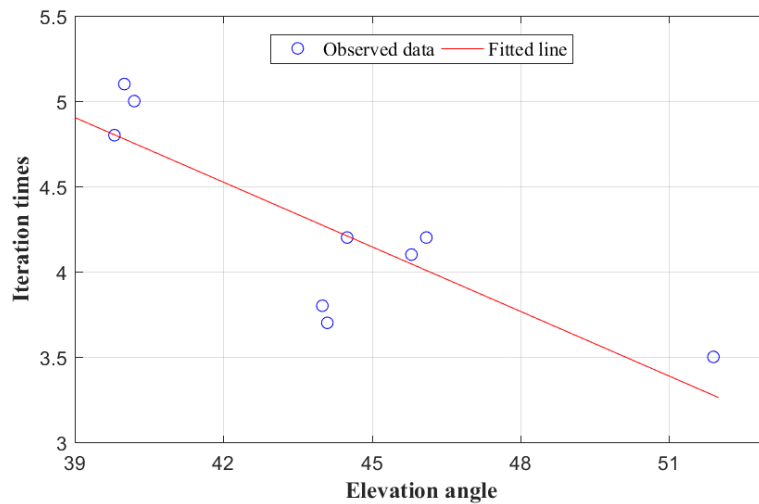
314 To analyse the performance of the multi-constellation GNSS troposphere tomography, the wet  
315 refractivity profile derived from nine schemes is first compared with the result from the radiosonde  
316 data thereat. The average RMS, Bias and MAE of wet refractivity difference between different  
317 schemes and radiosonde data over the experimental period are calculated (Table 8). As mentioned  
318 in Section 2, an iterative **procedure** is required to determine the weighting matrices of different  
319 equations in tomographic modelling. Therefore, the number of iterations and the average elevation  
320 angle of satellite signals for different schemes are also considered (Table 8). It can be observed from  
321 Table 8 that the average RMS, Bias, and MAE of different schemes are similar, which reflects the  
322 fact that the reconstructed wet refractivity profile obtained from different schemes applied at the  
323 radiosonde station have equivalent accuracy.

324 However, the number of iterations of various schemes are different when determining the weighting  
325 matrices of the different types of equations used in tomographic modelling. By analysing the  
326 relationship between the number of iterations and elevation angles over the tested period, a negative

327 linear relationship is found between two factors and the fitted data are presented in Figure 9. Such  
 328 a negative correlation reveals that the resolving time of tomographic modelling can be decreased  
 329 with multi-constellation GNSS observations, which is important in the real-time reconstruction of  
 330 atmospheric water vapour.

331 Table 8. Statistical result of average RMS, Bias, MAE, elevation angle and iteration times for  
 332 different schemes over the experimental period

Scheme	RMS	Bias	MAE	Iteration times	Elevation angle (°)
G-14	9.78	1.54	7.12	4.8	39.8
C-14	9.77	1.55	7.14	3.5	51.9
R-14	9.79	1.64	7.15	5.0	40.2
E-14	9.76	1.66	7.14	4.2	44.5
GC-14	9.76	1.54	7.11	4.1	45.8
GR-14	9.75	1.52	7.10	5.1	40.0
CR-14	9.78	1.56	7.14	4.2	46.1
GCR-14	9.76	1.55	7.09	3.8	44.0
GCRE-14	9.75	1.55	7.10	3.7	44.1



333

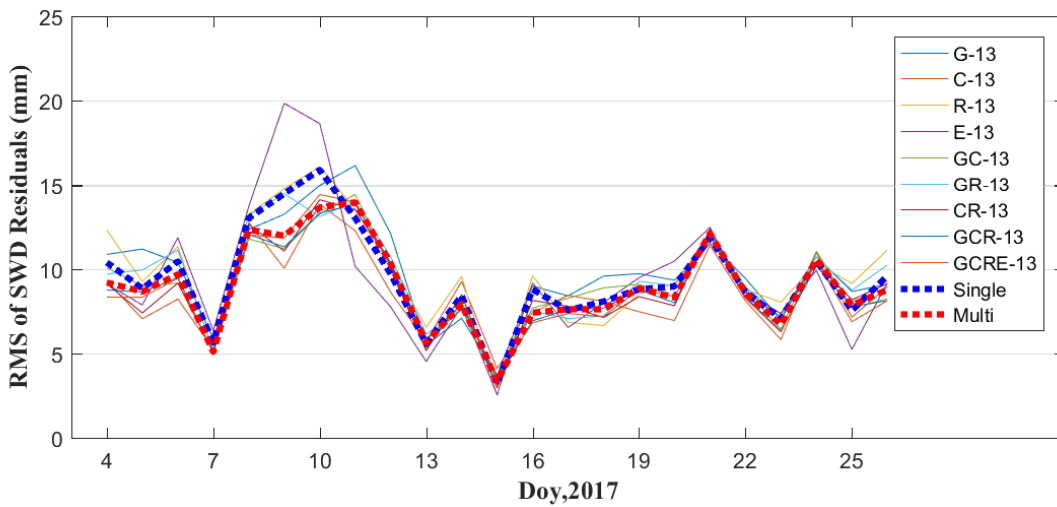
334 Figure 9. Relationship between iteration times and elevation angle during the experimental period

335

336 As mentioned above, the accuracy of different schemes evaluated for the location of radiosonde  
 337 cannot represent the tomographic quality across the entire region, therefore, a further comparison is  
 338 carried out using only thirteen GNSS stations in the network except for station HKSC. The slant  
 339 wet delays of station HKSC, estimated using multi-GNSS PPP software, are compared with the  
 340 calculated SWDs derived from different schemes. Figures 10 and 11 show the average RMS and  
 341 MAE of SWD residuals on each day during the experiment, where the blue dashed line represents  
 342 the average of RMS and MAE obtained from schemes G-13, C-13, R-13, and E-13, while the red  
 343 dashed line represents the average of RMS and MAE obtained from schemes GC-13, GR-13, CR-  
 344 13, GCR-13, and GCRE-13. From those two Figures, it was found that the reconstructed quality of  
 345 atmospheric wet refractivity field data for the entire region using multi-constellation GNSS  
 346 observations has been slightly improved when compared to that using single-constellation GNSS  
 347 data. By analysing the statistical results pertaining to different schemes (Table 9) it was found that,  
 348 compared to the single-constellation GNSS troposphere tomography, RMS accuracy of the multi-

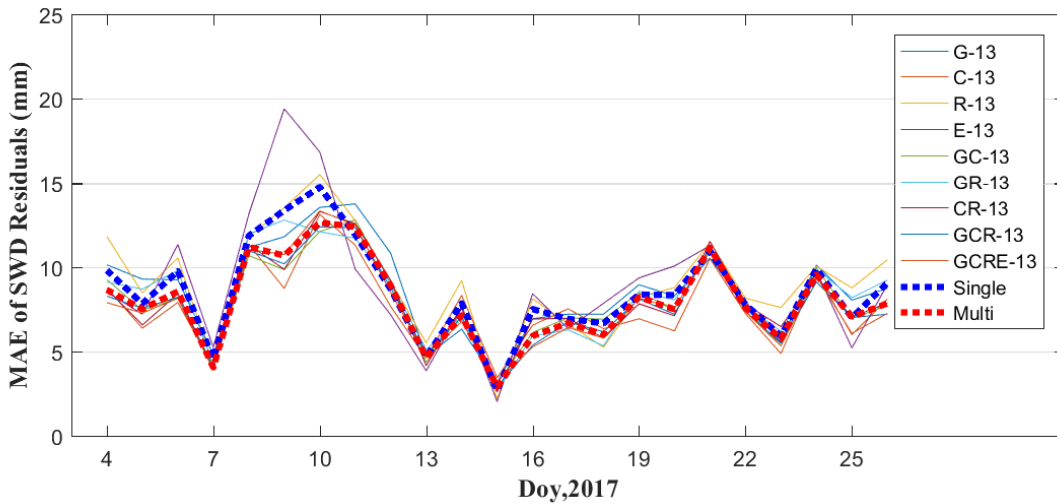
349 constellation GNSS troposphere tomography improved by about 10%.

350



351

352 Figure 10. Average RMS of SWD residuals for different schemes over the experimental period



353

354 Figure 11. Average MAE of SWD residuals for different schemes over the experimental period

355 Table 9. Statistical result of RMS, Bias and MAE of SWD residuals from different schemes over  
356 the experimental period

Scheme	RMS	Bias	MAE
G-13	9.83	6.71	8.62
C-13	8.58	6.34	8.58
R-13	9.05	7.65	9.05
E-13	9.41	7.62	8.83
GC-13	9.03	6.44	7.96
GR-13	9.40	6.66	8.28
CR-13	8.89	6.78	7.96
GCR-13	8.78	6.38	7.77
GCRE-13	8.75	6.36	7.73

357



## 358 **6 Conclusion**

359 The observed multi-constellation GNSS (GPS, BeiDou, GLONASS, and Galileo) observations have  
360 been used to investigate the importance and influence of station density and multi-GNSS  
361 constellation data on troposphere tomography. The SWDs of fourteen GNSS stations in a network  
362 in Hong Kong are estimated using the multi-constellation GNSS PPP software.

363 For GNSS troposphere tomography, the horizontal resolution of voxels is first determined according  
364 to the number of voxels and the coverage rate of GNSS stations located in the bottom layer. A  
365 comparative experiment using single/multi-constellation GNSS data derived from different numbers  
366 of stations revealed that increasing the station density improved the quality of tomographic results  
367 with the RMS accuracy of SWDs residuals increasing by about 16% when compared to the result  
368 of using multi-constellation GNSS troposphere tomography. In addition, compared to the single-  
369 constellation GNSS observations, troposphere tomography using multi-constellation GNSS data can:  
370 (1) reduce the resolving time when determining the weighting matrices of different equations used  
371 in tomographic modelling, which has practical significance for the real-time reconstruction of  
372 atmospheric water vapour profiles; and (2) improve the quality of tomographic results to a certain  
373 extent.

374 **The upcoming full operability of the multi-constellation GNSS** is expected to increase the number  
375 of SWDs used for troposphere tomography. Although the improvement of reconstructed results is  
376 not as expected, it was mainly determined by the spatial distribution of GNSS stations, multi-  
377 constellation GNSS troposphere tomography is also worth studying, especially for potential  
378 application of this technique in real-time atmospheric water vapour reconstruction.

379

380 **Acknowledgments:** The authors thank **IGRA** (Integrated Global Radiosonde Archive) for providing  
381 the radiosonde data. The Lands Department of HKSAR and Hong Kong Observatory are also  
382 acknowledged for providing GNSS and the corresponding meteorological data. This work is funded  
383 by the State Key Program of National Natural Science Foundation of China (Grant No. 41730109).

384

385 **Conflicts of Interest:** The authors declare no conflict of interest.

386

## 387 **References**

388 [1] Bartlett, M. S.: Properties of Sufficiency and Statistical Tests. In Proc. R. Soc. London A 160,  
389 268-282, 1937.

390 [2] Bender M., and Raabe A.: Preconditions to ground based GPS water vapour tomography  
391 *Annales geophysicae*, 25(8): 1727-1734, 2007.

392 [3] Bender, M., Dick, G., Ge, M., Deng, Z., Wickert, J., Kahle, H. G., Raabe, A., and Tetzlaff.:  
393 Development of a gnss water vapour tomography system using algebraic reconstruction techniques.  
394 *Advances in Space Research*, 47(10), 1704-1720, 2011.

395 [4] Bender, M., Stosius, R., Zus, F., Dick, G., Wickert, J., and Raabe, A.: GNSS water vapour  
396 tomography—Expected improvements by combining GPS, GLONASS and Galileo observations.  
397 *Advances in Space Research*, 47(5), 886-897, 2011.

398 [5] Benevides, P., Catalao, J., and Miranda, P. M. A.: On the inclusion of gps precipitable water  
399 vapour in the nowcasting of rainfall. *Natural Hazards & Earth System Sciences*, 3(6), 3861-3895,

400 2015a.

401 [6] Benevides, P., Nico, G., Catalao, J., and Miranda, P.: Can Galileo increase the accuracy and  
402 spatial resolution of the 3D tropospheric water vapour reconstruction by GPS tomography? In  
403 Geoscience and Remote Sensing Symposium (IGARSS), 2015 IEEE International, 3603-3606,  
404 2015b.

405 [7] Benevides, P., Nico, G., Catalão, J., and Miranda, P. M. A.: Analysis of galileo and gps  
406 integration for gnss tomography. *IEEE Transactions on Geoscience & Remote Sensing*, 55(4), 1936-  
407 1943, 2017.

408 [8] Benevides, P., Catalao, J., and Nico, G.: Inclusion of high resolution MODIS maps on a 3D  
409 tropospheric water vapor GPS tomography model. *Remote Sensing of Clouds and the Atmosphere*.  
410 International Society for Optics and Photonics, 9640, 96400R-1-96400R-13, 2015.

411 [9] Bi, Y., Mao, J., and Li, C.: Preliminary results of 4-D water vapor tomography in the  
412 troposphere using GPS. *Advances in atmospheric sciences*, 23(4), 551-560, 2006.

413 [10] Champollion, C., Masson, F., Bouin, M. N., Walpersdorf, A., Doerflinger, E., Bock, O., and  
414 Van Baelen, J.: GPS water vapour tomography: preliminary results from the ESCOMPTE field  
415 experiment. *Atmospheric research*, 74(1), 253-274, 2005.

416 [11] Chen, B. Y., and Liu, Z. Z.: Voxel-optimized regional water vapor tomography and comparison  
417 with radiosonde and numerical weather model. *Journal of Geodesy*, 88(7), 691-703, 2014.

418 [12] Crespi, M. G., Luzietti, L., and Marzario, M.: Investigation in gnss ground-based tropospheric  
419 tomography: benefits and perspectives of combined galileo, glonass and gps constellations.  
420 *Geophysical Research Abstracts*, 10, EGU2008-A-03643, 2008.

421 [13] Dong, Zhounan, and Shuanggen Jin. "3-D water vapor tomography in Wuhan from GPS, BDS  
422 and GLONASS observations." *Remote Sensing 10.1* (2018): 62.

423 [14] Flores, A., Ruffini, G., and Rius, A.: 4D tropospheric tomography using GPS slant wet delays.  
424 *Annales Geophysicae*, 18(2), 223-234, 2000.

425 [15] Guo, J., Yang, F., Shi, J., and Xu, C.: An Optimal Weighting Method of Global Positioning  
426 System (GPS) Troposphere Tomography. *IEEE Journal of Selected Topics in Applied Earth  
427 Observations and Remote Sensing*, 9(12), 5880-5887, 2016.

428 [16] Liu, Z., Wong, M. S., Nichol, J., and Chan, P. W.: A multi-sensor study of water vapour from  
429 radiosonde, MODIS and AERONET: a case study of Hong Kong. *International Journal of  
430 Climatology*, 33(1), 109-120, 2013.

431 [17] Niell, A. E., Coster, A. J., Solheim, F. S., Mendes, V. B., Toor, P. C., Langley, R. B., and Upham,  
432 C.: A. Comparison of measurements of atmospheric wet delay by radiosonde, water vapor  
433 radiometer, GPS, and VLBI. *Journal of Atmospheric and Oceanic Technology*, 18(6), 830-850, 2001.

434 [18] Nilsson, T., and Gradinarsky, L.: Water vapor tomography using gps phase observations:  
435 simulation results. *IEEE Transactions on Geoscience & Remote Sensing*, 44(10), 2927-2941, 2006.

436 [19] Notarpietro, R., Cucca, M., Gabella, M., Venuti, G., and Perona, G.: Tomographic  
437 reconstruction of wet and total refractivity fields from gnss receiver networks. *Advances in Space  
438 Research*, 47(5), 898-912, 2011.

439 [20] Radon, J.: Über die bestimmung von funktionen durch ihre in-te-gral-werte längs gewisser  
440 mannigfaltigkeiten. *Computed Tomography*, 69, 262-277, 1917.

441 [21] Rohm, W., and Bosy, J.: Local tomography troposphere model over mountains area.  
442 *Atmospheric Research*, 93(4), 777-783, 2009.

443 [22] Skone, S., and Hoyle, V.: Troposphere modeling in a regional gps network. *Positioning*, 4(1&2),

444 230-239, 2005.

445 [23] Troller, M., Bürki, B., Cocard, M., Geiger, A., and Kahle, H. G.: 3-d refractivity field from gps  
446 double difference tomography. *Geophysical Research Letters*, 29, 2149–2152, 2002.

447 [24] Troller, M., Geiger, A., Brockmann, E., Bettems, J. M., Bürki, B., and Kahle, H. G.:  
448 Tomographic determination of the spatial distribution of water vapor using GPS observations.  
449 *Advances in Space Research*, 37(12), 2211-2217, 2006.

450 [25] Wang, X., Dai, Z., Wang, L., Cao, Y., and Song, L.: Preliminary Results of Tropospheric Wet  
451 Refractivity Tomography Based on GPS/GLONASS/BDS Satellite Navigation System. In *China  
452 Satellite Navigation Conference (CSNC) Proceedings: Volume I*, 1-7, 2014.

453 [26] Yao, Y. B., and Zhao, Q. Z.: A novel, optimized approach of voxel division for water vapor  
454 tomography. *Meteorology and Atmospheric Physics*, 129(1), 57-70, 2016a.

455 [27] Yao, Y. B., and Zhao, Q. Z.: Maximally Using GPS Observation for Water Vapor Tomography.  
456 *IEEE Transactions on Geoscience and Remote Sensing* 54(12), 7185-7196, 2016b.

457 [28] Yao, Y. B., Zhao, Q. Z., and Zhang, B.: A method to improve the utilization of GNSS  
458 observation for water vapor tomography. *Annales Geophysicae*, 34(1), 143-152, 2016.

459 [29] Zhao, Q. Z., Yao, Y. B., Cao, X. Y., Zhou, F., and Xia, P.: An optimal tropospheric tomography  
460 method based on the multi-GNSS observations. *Remote Sensing*, 10(2), 1-15, 2018.

461 [30] Zhao Q. Z., and Yao Y. B.: An improved troposphere tomographic approach considering the  
462 signals coming from the side face of the tomographic area. In *Annales Geophysicae*, 35(1), 87-95,  
463 2017.